CHALMERS
UNIVERSITY OF TECHNOLOGY

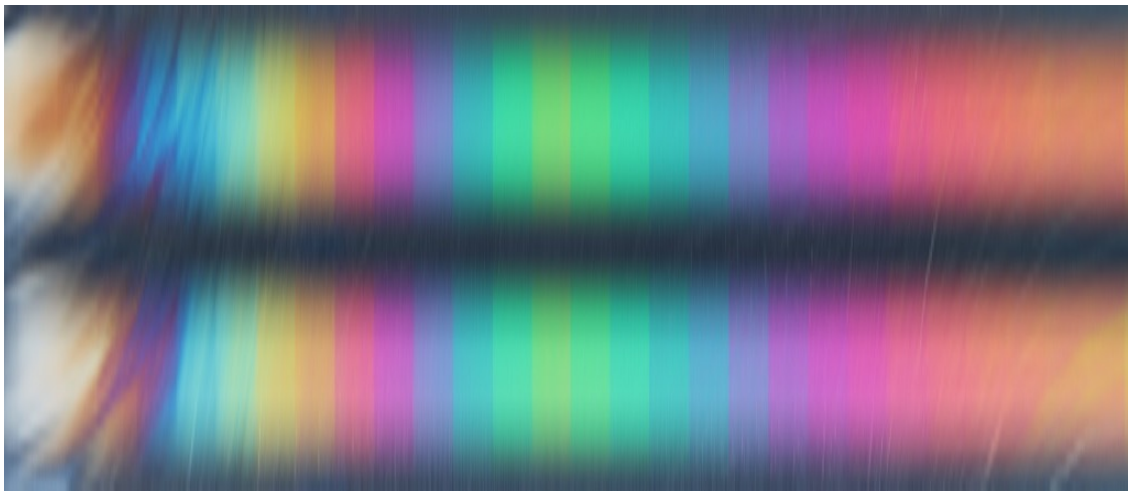

# Shear-induced orientation and yielding of Cellulose nanocrystal suspensions: A Rheo-PLI study

Master's thesis in Innovative and Sustainable Chemical Engineering

VIHANGI VINODYA

DEPARTMENT OF INDUSTRIAL AND MATERIALS SCIENCE

CHALMERS UNIVERSITY OF TECHNOLOGY
Gothenburg, Sweden 2024
www.chalmers.se

Master's thesis 2024

# Shear-induced orientation and yielding of Cellulose nanocrystal suspensions: A Rheo-PLI study

VIHANGI VINODYA


CHALMERS
UNIVERSITY OF TECHNOLOGY

Department of Industrial and Materials Science
Chalmers University of Technology
Gothenburg, Sweden 2024

Shear-induced Orientation and Yielding of Cellulose nanocrystal suspensions: A Rheo-PLI study

VIHANGI VINODYA



Supervisor: Ases Akas Mishra, Marko Bek, Department of Industrial and Materials Science
Examiner: Prof. Roland Kádár, Department of Industrial and Materials Science

Master's Thesis 2024
Department of Industrial and Materials Science
Chalmers University of Technology
SE-412 96 Gothenburg
Telephone +46 31 772 1000

Cover: PLI Image corresponds to CNC 6wt% suspension subjected to thixotropy test with shear rate range 0.1-100Pa

Typeset in LaTeX
Printed by Chalmers Reproservice
Gothenburg, Sweden 2024

Shear-induced Orientation and Yielding behavior of Cellulose nanocrystals
VIHANGI VINODYA
Department of Industrial and Materials Science
Chalmers University of Technology

# Abstract

This thesis presents an investigation of the shear-induced orientation and yielding behavior of CNC water suspensions by employing a Rheo-PLI technique. Cellulose is a structural protein found in plants and algae and plants produce them through synthesis.CNC has demonstrated potential in numerous applications due to its properties such as high mechanical strength, higher crystallinity, high aspect ratio, and optical properties. They are usually using in automotive industries,pharmaceutical industry, reinforcements in fillers and much more.The orientation and its microstructure highly impact to optical and mechanical properties. This study includes the preparation of CNC suspensions and analyze their rheological properties from rheological tests combined with polarized light imaging. In this study we combined the rheological tests with the polarized light imaging technique inorder to examine the yielding and shear-induced orientation of CNC structures in their suspension. We have performed hysteresis loop tests to investigate the thixotropic behavior, oscillatory tests to analyze the viscoelastic behavior, creep tests to examine the stability of CNC suspensions, and Yield stress to determine yielding behavior.

Keywords:CNC, Rheo- PLI, Shear Orientation, Yielding behavior of CNC,Viscoelasticity

# Acknowledgements

I would like to thank my examiner Prof.Roland Kadar for providing the opportunity to conduct this project, support, insights, and guidance throughout the project.

Also, I would like to express my gratitude to my supervisors Ases Akas Mishra and Marko Bek for their guidance, encouragement, and immense support throughout the project. I am so grateful for the effort and time they and valuable insights provided throughout the project work.

Also, I would like to thank everyone at the Rheology and Processing lab for helping in this project and providing me with more ideas. A special thanks to Manoj Chandregowda for helping me with sample preparations and company during the project.

Lastly, I want to thank my family and friends for their support, love and encouragement throughout in this journey

Vihangi Vinodya, Gothenburg,June 2024

# List of Acronyms

Below is the list of acronyms that have been used throughout this thesis listed in alphabetical order:

| | |
|---|---|
| PLI | Polarized Light Imaging |
| POM | Polarized Optical Microscopy |
| CNC | Cellulose Nano Crsytals |
| LC | Liquid Crystalline |
| SAOS | Simple Amplitude Oscillatory Shear |
| MAOS | Medium Amplitude Oscillatory Shear |
| LAOS | Large Amplitude Oscillatory Shear |
| fps | frames per second |
| f | frequency |
| RPM | Revolutions per minute |

# Nomenclature

Below is the nomenclature of parameters that have been used throughout this thesis.

## Parameters

| | |
|---|---|
| $\sigma$ | Shear stress |
| $\dot{\gamma}$ | Shear rate |
| $\eta$ | Shear Viscosity |
| $L_{rad}$ | Radial distance of observation region |
| $L_{arc}$ | Distance of arc A-B |
| $t$ | Time in seconds |
| $G'$ | Storage Modulus |
| $G''$ | Loss Modulus |
| $\gamma(\%)$ | Shear strain amplitude |

# Contents

# List of Figures

# 1
# Introduction

Cellulose nanocrystals are characterized as stiff rod-like particles possessing crystalline structures, demonstrating specific liquid crystalline properties,higher mechanical strength, and storage modulus.[2] Combining rheology with optical techniques allows the analysis of rheological measurements and simultaneous observation of CNC structure development in their suspensions. The study focuses on the investigation of rheological properties of Cellulose nanocrystal suspensions in combined observation of shear-induced orientation and yielding behavior.

## 1.1 Cellulose nanocrystal structure and phase behavior in suspensions

Cellulose nanocrystals are obtained from cellulose microfibrils by employing a combination of chemical, mechanical, and enzymatic treatments leading to the extraction of high crystalline areas.[1]. The source of the cellulose microfibrils and the hydrolysis parameters impact the variations of the dimensions of CNC including length and width. The dimensions of CNCs are typically available within the range of about 3 – 5 nm in diameter and 100 – 300 nm in length.[3] Furthermore, individual particles form larger clusters in suspensions due to the formation of interparticle attractions with water suspensions through hydrogen bonding.[4] Strong acid hydrolysis is commonly used to eliminate amorphous regions from, leading to the formation of rod-shaped CNCs with high crystallinity. CNCs forms hierarchical structures that exhibit optical active properties in water suspensions ranging from nano to micro scale.[1]

Cellulose Nanocrystals (CNC) self-assemble into a cholesteric liquid crystal (LC) phase, forming a spiral structure with layers oriented in the xy plane.[5] CNCs have the ability to form numerous structures in their suspensions, isotropic, biphasic, chiral nematic, and liquid crystalline phases. The isotropic phase is observed at low CNC concentrations where CNCs shows a random arrangement in the suspension.[6, 7] The isotropic phase forms a biphasic phase when it reaches a specific concentration. With the increase of CNC concentration leads to the formation of chiral nematic structures in the liquid crystalline phase which has the ability to polarize light through its helical structure. The chiral nematic structures loses their stability, leading to the formation of a gel phase once high concentrations are reached.[8, 9]

The helical pitch (P) of CNC liquid crystal structure determines the wavelength of reflected light, influencing color changes. This P can be controlled by factors like concentration of nanocrystals and external conditions. The cholesteric phase demonstrates birefringence and optical activity as a result of its chiral structure along its helix axis, with helical pith (P) directly impacting the color of reflected light. The birefringence, chiral structure and templating potentials observed in CNC suspensions are preserved even after the suspensions dried to form CNC films. This property is essential for applications that require unique optical characteristics of CNC-based liquid crystals.[6, 10, 11]

## 1.2 Rheo-PLI technique

Combination of optical visualization techniques and rheological analysis helps in understanding how the phase transitions, microstructure and rheological properties are interrelated.Polarized light Imaging (PLI) is one of the most commonly used methods to analyze the rheo - optical properties of optically active suspensions.[12, 13] Rheology can be referred as a comprehensive measurement tool that capture and analyze the behavior of materials at all levels of their material hierarchy. Combining rheological methods with other analytical technique provides a comprehensive understanding of the dynamics of material flow.[14]

Polarized light imaging identifies orientation changes by visualizing polarizing patters which evolve in cellulose nanocrystal suspensions in bulk flow. When the CNC suspensions are placed in between an analyzer and a polarizer, a colorful pattern can be observed in the observable length scale. Displayed colors are identified as the birefringence pattern or polarization and demonstrates the organizational arrangement in the suspension.[15, 16]

Chiral periodicity is defined as the repeating pattern in materials with twisted structure that can be validated by fingerprint pattern with lines which implies the pitch of chiral order. Here pitch denotes the distance over the twisted structure that reoccurs. The chiral periodicity forms a layered pattern in CNC material where layers are made on the basis of chiral order indicating the periodicity of the layers.[17, 18] The presence of fingerprint patterns and chiral periodicity provides valuable insights into the structural arrangement of CNC suspension. It helps to understand the alignment and orientation of CNC in material.The patterns of birefringence observed in PLI experiments occurs due to the presence of mesogens distributed unidirectionally in a polydomain structure which aligns towards a nematic alignment under the influence of sufficiently high shear rates.[19]

Haywood et al.(2017) investigated the flow alignments, microstructural relaxation, and liquid crystalline behavior of CNC using Rheo–optics and microspectrophotometry.[20] Recently Kadar et al.(2023) examined the effect of surface charge on percolation, phase behavior, and gel point of cellulose nanocrystal (CNC) relevant to their nonlinear rheological responses using polarized light imaging(PLI).[21] The results highlighted that microstructural changes occur with nano-linear changes in CNC sus-

pensions, emphasizing the sensitivity of nonlinear parameters in different phases of CNC. Kadar et al.(2022) also examined the nonlinear rheological analysis employing polarized light imaging, which can differentiate between CNC phases like isotropic, biphasic, and liquid crystalline phases.[22] In another study, kadar et al.(2021) highlighted that Rheology coupled with spectroscopy, scattering, and optical techniques plays a pivotal role in the characterization of CNC hierarchical levels that span from nano to micro scale.[23] In his other study, he has investigated the thixotropic behavior of CNC suspensions by combining rheology tests with rheo-PLI.[24]Several rheological tests like Creep, ramped hysteresis loop, dynamic sweep, and thixotropy with rheo – PLI have been employed to examine the distinct contributions of various hierarchical levels of CNC on their thixotropy

## 1.3 Rhelogical Measurements

The thixotropy behavior of materials is characterized as an increase of viscosity under static conditions and a decrease of viscosity when subjected to constant shear stress or rate.[25] The evaluation of thixotropy in rheology involves assessing the structural destruction and recovery of materials under shear stress or rate.[26] Similar to the yield stress scenario, researchers have believed that the thixotropic nature is caused due to the presence of material structure. In these kinds of materials, the material takes time for the structure to break down under shear stress(rate), similarly, it takes time to rebuild the initial structure upon the release of shear stress(rate).[27] Because of this similarity, Most of the researchers have considered thixotropy and yield stress as two phenomena with same origin and they are interconnected. The microstructural origins of thixotropic behavior depend on the Brownian motion, intermolecular forces, and hydrodynamic interactions. Hysteresis behavior in thixotropy is characterized by material exhibiting distinct properties when exposed to increasing and decreasing shear rates resulting in loop-like configurations in rheological experiments.[28, 29]

Creep tests in rheology entail applying constant stress or load to materials over time to examine their deformation characteristics. These tests provide insights about the mechanical properties and long-term stability of materials when they are subjected to understanding how materials make deformations when subjected to constant stress over a long time.[30, 31, 32] Mohsin Jaber Jaweej et al.(2014) examined the creep behavior of Carbon Nanotube composite columns and the results showed that the higher fiber concentrations exhibit higher creep resistance.[33] Yi Luen Li et al.(2011) investigate the impact of surface modification of carbon nanotubes (CNT) on its electrical conductivities and mechanical properties. The research focused on analyzing the creep behaviors of CNTs/epoxy resins/CF under different stresses, temperatures, orientations of fiber, and humidities. Viscosity increases for stresses below yield stress promoting restructuring outweighs over destruction. On the other hand, Viscosity decreases when applied stress is higher than yield stress due to the destruction of the microstructure.[34, 24]

Oscillatory shear experiments are widely employed in rheology to study the linear

and non-linear responses of fluids during cyclic deformation.[35] Large Amplitude Oscillatory shear(LAOS), Medium Amplitude Oscillatory Shear (MAOS), and Small Amplitude Oscillatory Shear (SAOS) are tests used to analyze viscoelastic materials and provide perspectives about materials under varying strains.[36] LAOS tests are employed to analyze and characterize the nonlinear viscoelastic nature of complex fluids.[37] On the other hand, SAOS is usually used to analyze the linear viscoelasticity of complex fluids. It provides convenient and useful rheological characterization since the SAOS test assumes that the response of material remains within the linear range. Furthermore, MAOS is a subset of SAOS and provides valuable insights about materials and intrinsic nonlinearities.[38, 39] Recently several researches have been conducted on oscillatory tests of carbon nanocrystals. Danesh et al.(2020) conducted a rheological study of the behavior of CNC employing an oscillatory test, identifying two different yield stresses.[40] Wonjo et al.(2019) examined the behavior of CNC with a focus on fundamental characteristics of rod-shaped suspensions that orient themselves underflow and display liquid crystal properties at rest, even for a certain range of concentration.[41] This research illustrates the importance of performing oscillatory tests in understanding the rheological properties and behavior of CNC under numerous conditions.

Yield stress is the stress necessary to apply on a sample to initiate a deformation. If the applied stress is below the yield stress, the sample undergoes elastic deformation, while above the yield stress sample flows like a liquid.[42, 43] Many researchers have conducted studies on the yield stress of CNC based on different methodologies and conditions. Behzad Zakani  Grecov et al.(2020) investigated the yielding behavior of highly concentrated CNC suspensions using different rheological experiments and they obtained clear viscosity bifurcation and the true yield stress.[44] One of the easiest and widely used methods for determining the yield stress of a material is to conduct a shear stress ramp test and identify the corresponding stress that viscosity reaches the peak point. The material is subject to elastic deformation before it reaches the viscosity peak where the sample undergoes stretching. When the material reaches the peak point elastic structure breaks down and the material starts to flow[40, 43].

## 1.4 Aim of the study

The aim of the study is to investigate the shear-induced orientation and yielding behavior of CNC water suspensions by employing a Rheo-PLI technique. This includes the preparation of CNC suspensions and analyze their rheological properties from rheological tests combined with polarized light imaging.POM was used to analyse the structure of CNC in suspensions. Here we have performed hysteresis loop tests to investigate the thixotropic behavior, oscillatory tests to analyze the viscoelastic behavior, creep tests to examine the stability of CNC suspensions, and Yield stress to determine yielding behavior.

# 2

# Theory

This chapter includes the theoretical aspects related to rheological measurements involved in this study, the polarization technique, and the CNC structure development in their suspensions. Under rheological measurements, we have discussed linear viscoelasticity, Dynamic Oscillatory test, thixotropy, and yield stress. In addition types of polarization and a brief discussion about linear cross-polarization.Also the structure development in CNC suspensions, length scales involved in structures, and how shear affects on structures.

## 2.1 Rheological Measurements

### 2.1.1 Linear viscoelasticity

Viscoelasticity is a rheological property of materials that demonstrates both viscous and elastic properties. Viscoelasticity is also referred to as elasticity when undergoing deformation. Viscous substances such as honey show resistance to shear flow.[45] The viscous component refers to the dissipation ability while the elastic component refers to the material's ability to experience reversible elastic deformation. The dynamic oscillatory test is one of the most common rheological method to measure the linear viscoeslaticity of materials. The storage modulus (G') measures the deformation energy retained while the loss modulus (G") measures the energy dissipated from the material[46].

#### 2.1.1.1 Dynamic Oscillatory test

The dynamic oscillatory test involves applying a sinusoidal deformation on a material and measuring the subsequent mechanical response over time. This test is the most common method to measure the viscoelasticity of a material[47]. The viscoelastic behavior of a material can be quantified by two measures, viscous loss modulus G" and the elastic storage modulus G'. If the storage modulus is higher than the loss modulus (G' > G") of the material, it shows a gel-like behavior; conversely, if G" > G' material shows a liquid-like behavior.[48]. Oscillatory tests can be categorized into two main regions according to their linearity of response. As shown in Figure 2.1,the region with linear viscoelastic behavior, where both dynamic responses remain independent of applied strain amplitude is defined as SAOS (small amplitude oscillatory shear),while the non-linear region is defined as LAOS(large amplitude oscillatory shear).[49, 50].

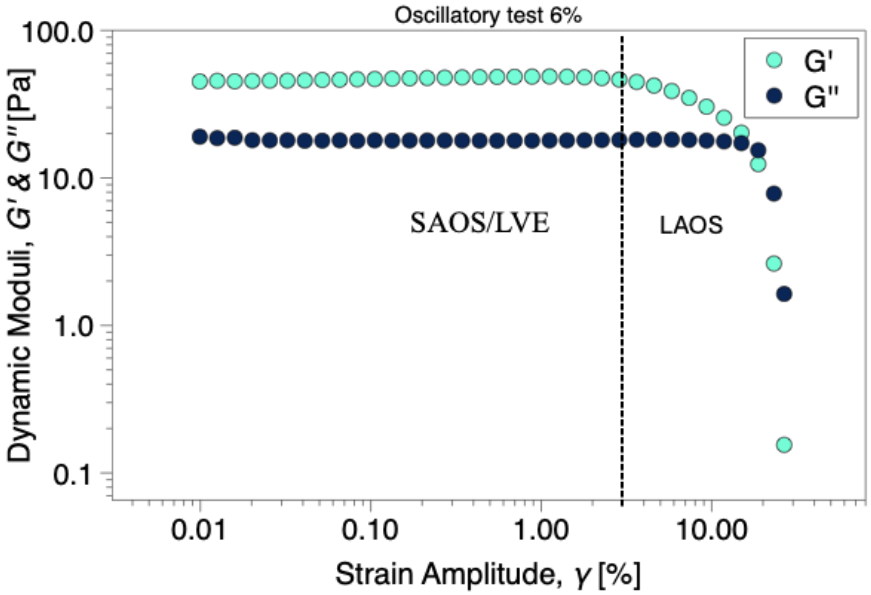


**Figure 2.1:** Oscillatory shear strain sweep

### 2.1.2 Thixotropy Test

The thixotropy phenomenon plays an important role as a quality aspect in various materials, for example, coatings and paints. It affects the spreading of paint and ensures a uniform thickness. Thixotropy yield stress materials exhibit a behavior that depends on the flow history[51]. Upon the application of shear rate on thixotropic material, a continuous reduction of viscosity with time followed by a recovery of viscosity can be observed. Numerous test methods are used to measure the thixotropic behavior of a material. Some of the test methods are mentioned below.[52]

#### 2.1.2.1 Hysteresis Loop Test

The most simplest test method to determine thixotropic behavior is the so-called ' Hysterius Loop Test'. It involves when the material is subjected to a cyclic shear process, usually a series of ramp up and downward of shear rate in stepwise[53]. When the induced shear stress is plotted with the applied shear rate, the loading and unloading curves do not overlap as shown in the figure 2.2. The structure of the material destructs and builds up with the increase and decrease of shear rate respectively[54]. The area enclosed between the upward and downward provides a quantification of thixotropy. The amplitude of hysteresis provides insights into the significance of dependence on the shear history of the material. The induced shear stress and magnitude vary based on the time step size at different shear rates[55].

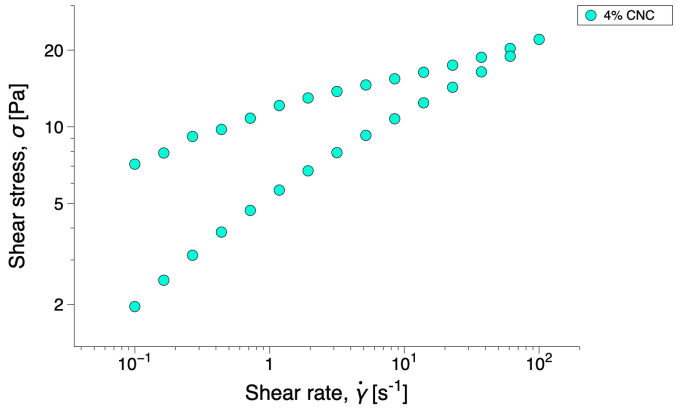


**Figure 2.2:** Hysteresis loop curve

### 2.1.3 Yield Stress Test

The yield stress is the minimum shear stress value below which a material shows fluid-like behavior and above behaves as a fluid. Multiple methods are used to determine the yield stress of a material, some of which are explained below[56].

#### 2.1.3.1 Shear rate Controlled steady shear test

The conventional approach for determining the yield stress of material was fitting shear stress vs shear rate data for theoretical models and extrapolating to zero shear rates. The shear rate is increased in this test and shear stress is measured for each shear rate(shear rate controlled steady shear stress). In this method, a shear rate is applied to the material. Among these models, the simplest one is the Bingham model, commonly used to characterize the flow behavior of Newtonian fluids[57].

Herschel – Bulkley model is another yield stress model, that characterizes non-Newtonian behavior exhibited after yielding. This model elucidates the rheological behavior of a material with yield stress as well as shear thinning or thickening behavior[58].

n is the shear thinning index and K is the consistency. The second term denotes the extent to which the material exhibits shear thinning (n<1) or shear thickening(n > 1). There are two distinct yield stresses for any fluid. The stress required to overcome plastic deformation is known as static yield stress while the stress required to sustain the plastic deformation is known as dynamic yield stress. The static yield stress of the flow curve is where it intersects the y-axis when the curve is generated by gradually increasing the shear rate, while the dynamic shear rate is acquired by decreasing the shear rate[59, 60].

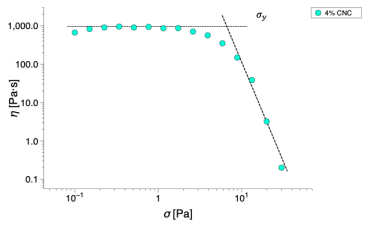


**Figure 2.3:** Shear controlled steady shear stress

### 2.1.4 Stress controlled steady shear stress

Stress-controlled steady shear stress test is another method to measure static stress where viscosity is measured with an increase of shear stress. Viscosity reduces due to the plastic deformation that occurs in the material. Yield stress can be determined by locating the intersection point of the tangents of viscosity function[61].

## 2.2 CNC Structure and Phase behavior

CNC has the ability to self-assemble into various structures in their aqueous suspensions. At lower concentrations, isotropic domains can be observed with a random arrangement of CNC rods. With the increase in CNC concentrations,it leads to the formation of concentrated isotropic, biphasic and liquid crystalline domains. Due to the presence of hydroxyl groups on the surface of CNC rods, form interparticle attractions in water suspensions via hydrogen bonding[62, 63]. These interactions is a result of the attraction of hydrogen bonding and repulsion of electrostatic forces. These interactions result in multiple length scales of CN structures which span from nm to m length scales.CNC rods make liquid crystalline domains of micrometer range which consists of multiple rods. Application of shear leads the CNC structures to align towards the shear flow direction as shows in figure 2.4[64].

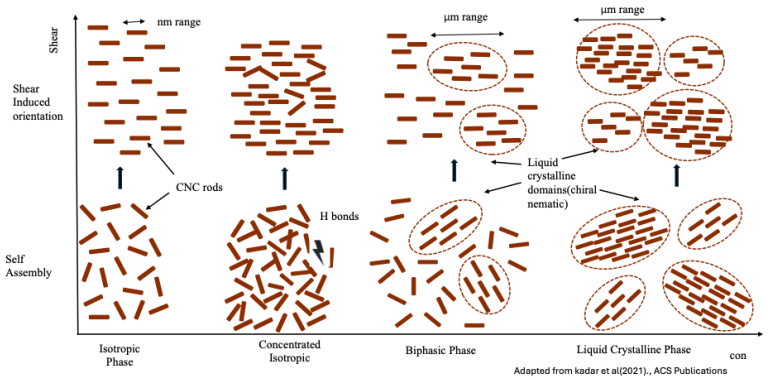


**Figure 2.4:** CNC structure and Phase behavior

## 2.3 Polarization

Light can be characterized as an electromagnetic wave with its electrical field oscillating perpendicular to the propagation direction. When the direction of the electrical field oscillates randomly with time, it is referred as unpolarized light. Most of the common light sources such as sunlight, halogen lighting, and incandescent lights emit unpolarized light. In contrast, when the direction of the light is well-defined it is referred to as polarized light[65, 66].

Polarized light can be mainly classified into three main types according to the orientation of the electric field. They are,

- Linear polarization: When the electric field of the light is directed towards the same plane of propagation direction
- Circular polarization: The electric field of light comprises of two perpendicular light components of equal magnitude, differing in phase by 90°. Consequently, the resultant electric field rotates around the propagation direction and it can be termed a right-hand or left-hand circular motion based on the direction of rotation
- Elliptical polarization: The elliptical path traced by the electric field of light occurs due to the combination of two linear components with varying amplitudes and phase differences that are not 90°[67, 68].

### 2.3.1 Linear Polarization

A linear polarizer allows the transmission of light with uniform vibration along a single plane and absorbs light that oscillates in the perpendicular plane. The characterization of a single plane or polarized light typically involves defining the vibration pattern. If the vibration occurs in a specific direction, the light can be referred as linearly polarized light.

A polarizer consists of two axes: The transmitting axis and the absorbing axis. The transmitting axis is commonly known as the 'polarization axis'. The light that passes through a single polarizer typically loses a minimum of 50% during transmission, which varies based on the quality and grade of the polarizer used and the requirements of polarization[69, 70].

When two linear polarizers cross at 90° with one another,it can result in blocking of light. This phenomenon is termed extinction. The ratio of transmission between two polarizers with axes parallel to the crossed axes is identified as the polarizer's efficiency. It is important to note that enhancing transmission does not necessarily result in increased efficiency due to the subsequent rise in extinction transmission.

When the isotropic region is viewed through the cross polarizers dark region can be observed since the light emitted from isotropic domains retains the polarizer it

has on entering. This light does not passes through the upper polarizer which results in a dark region. In contrast, anisotropic domains of chiral nematic structures exhibit colors due to the randomly oriented structures in the domains. The random orientation directions of chiral nematic structures are normally not perpendicular to the upper polarizer. Therefore, some rays pass through the upper polarizer and appear as different shades of colors.

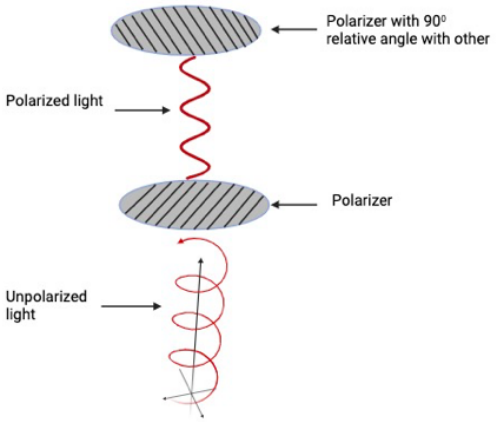


**Figure 2.5:** Cross Polarization

# 3
# Methods

This chapter focuses on steps involved with sample preparation of 4 and 6wt% of CNC concentrations, Rheo - PLI, and POM setup used for this study followed by the details on parameters and conditions involved with rheological tests[72].

## 3.1 Sample preparation and Experimental procedures

### 3.1.1 Sample Preparation

The required CNC powder(CelluForce NCC Montreal, Canada) to make CNC suspensions of 4 and 6wt% weight was measured and dispersed in tap water. Then mix the samples using an overhead mixer for 30 min at 2000 RPM. Samples were prepared within 48 hrs before the measurement and the mentioned preparation steps were followed similarly for all the samples because the preparation procedure can be affected by the rheological properties of the sample. These two suspensions were chosen to represent different phases of CNC suspensions. We hypothesize that the 4wt% represents the biphasic phase while 6wt% represents the liquid crystalline phase.

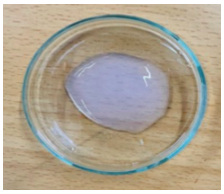

**Figure 3.1:** Sample of 4wt%

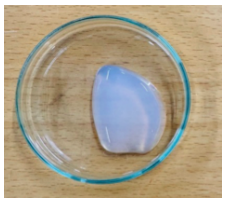

**Figure 3.2:** Sample of 6wt%

### 3.1.2 Experimental Setup of Rheo-PLI

Rheological experiments were carried out using the Anton Paar MCR 702 space rheometer featuring a glass parallel plate geometry (diameter 43 mm) with a measurement gap of 1mm. The tests were conducted in a single motor–transducer configuration. The setup includes a parallel plate geometry of (2R =) 43mm diameter with a measurement gap of 1mm. The outer area of the upper geometry and lower geometry were transparent(made of glass). An optical camera was placed below the lower plate as shown in figure 3.1. Two linear polarizers were positioned

below the lower plate and above the upper plate oriented at a relative angle of 90°. Two light sources were placed above the geometry on opposite sides as shown in the diagram(figure 3.1). To get a better light for the videos the intensities were adjusted as 25% and 50% for light A and B respectively.

Video recordings of rheo tests were conducted in HD format (1920 x 1080 pi) at 30fps (frames per second) using a 100mm macro lens together with a 25mm extension tube(Canon, Japan). The experimental area encompasses the 2nd half of a circle as shown in figure 3.1. All tests were performed at 23°C with the measurement plate temperature regulated by a Peltier system. An optical representation of the observation region with a sample at rest shown in Figure 3.1, and a corresponding representation of the observation region when a shear rate of 100 sample subjected to the thixotropy test is shown in Figure 3.1. The optical visualization was transformed into a space-time diagram using MATLAB in order to highlight the influence of deformation over arc A-B and radial deformation over line L with time on the material flow. The arc A – B and line L in optical visualization correspond to the verticle axis of the space-time diagrams as shown in Figure 3.1, which depicts the number of points over the arc[72].

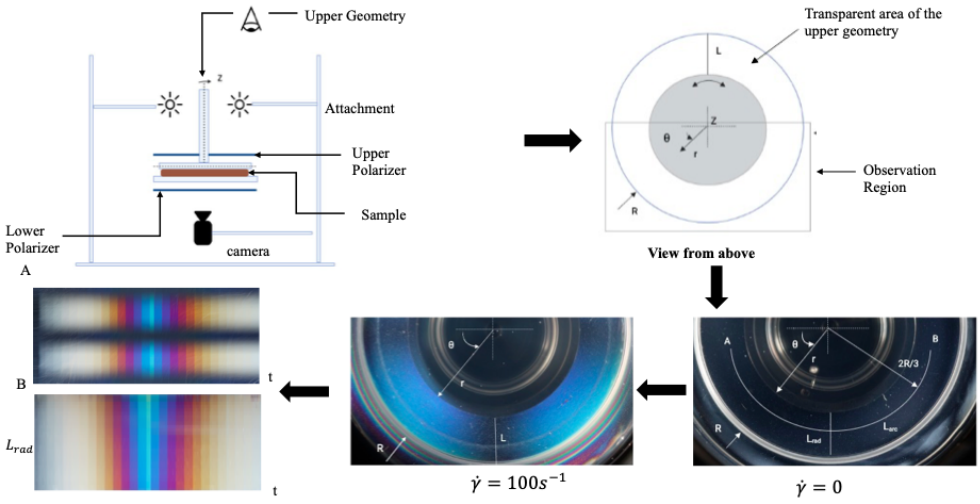


**Figure 3.3:** Experimental setup and optical visualization

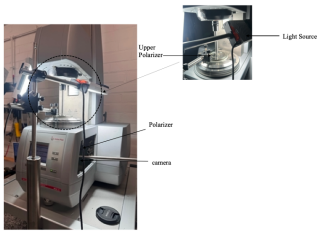


**Figure 3.4:** Rheo-PLI setup used for the study

### 3.1.3 Experimental Setup of Polarized Light Imaging

In this setup, the sample was placed in between two linear polarizers with a relative angle of 90°. A light source was placed below the lower polarizer and a dino-Lite optical camera was placed above the upper polarizers shown in figure 3.5. CNC structure of suspensions observed through the optical camera.

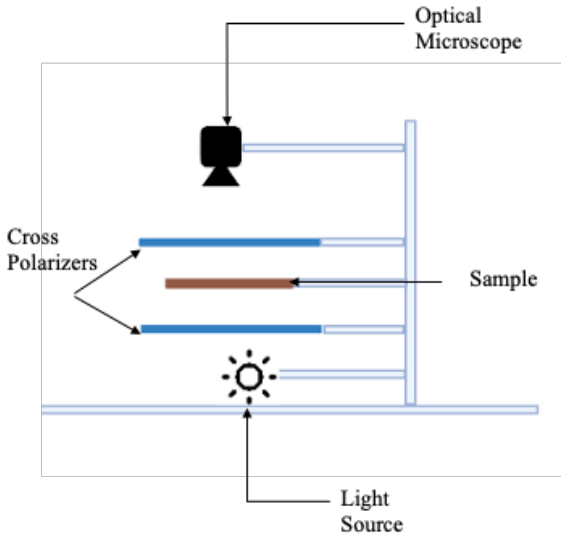


**Figure 3.5:** POM Setup

### 3.1.4 Methods

Four experimental techniques were used to study the rheological properties of CNC suspensions, hysteresis loop tests (to measure thixotropy), oscillatory tests, creep tests and yield stress tests.

The thixotropic behavior of CNC samples was measured through hysteresis loop tests. The shear rate was ramped upward and then ramped down. The applied shear rate increases in the range from 0.1 to 100 and decreases within the same range with a step size of 30s and 45s at each shear rate over 29 equal size time intervals. Both 4% and 6% CNC samples were tested with a time step size of the 30s and 45s at each shera rate, over the same shear rate range of 0.1 to 100. The shear stress was measured at each shear rate.

During creep tests, constant shear stresses of five values were imposed and transient viscosity was measured over 1000s. In this study, we applied the shear stresses that are greater than, less than,and near the yield stress. For 4% and 6% CNC concentration samples, we imposed constant shear stresses in the range of 0.1 – 10 Pa and 5 – 30 Pa respectively.

In dynamic oscillatory tests, storage and loss modulus were measured in time at a constant angular frequency of 1 Hz and shear strain amplitude range of 0.001% to 1000%. The visco-elastic behavior of CNC can be determined through this test.

Yield stress tests involved the application of stress-controlled steady shear stress to measure the viscosity function of the material.The measured yield stress of the samples was used to select the constant shear stresses for the creep tests.

Space-time diagrams were generated from the video recordings by extracting a single line pixel at a fixed position from each frame and assembling them into a new image. The created image has an x-axis aligned with the experimental time where the time interval between two pixels is t=$1/f_{\mathrm{acq}}$=0.033s and the y–axis denotes the number of points in arc A – B as shown in Figure 3.1.

# 4

# Results

This chapter presents the results and findings of this study.At the beginning, CNC phase behavior of 4wt and 6wt% has been discussed relative to the images obtained from POM. Detailed discussion on Rheo-PLI results of tests is discussed in the following section of the chapter.

## 4.1 Results and Discussion

### 4.1.1 CNC Phase behavior

POM images of 4 wt% and 6wt% CNC concentration samples at rest is shown in figure 4.1 and 4.2 respectively. Both suspensions show fingerprint patterns of chiral nematic structures. 4% shows lower fingerprint patterns when compared with 6% .4% sample also exhibits dark regions which is an indication of presence of isotropic domains as shows in figure 4.1. Therefore, it can concluded that 4% has a biphasic phase of CNC structure comprised of both isotropic and liquid crystalline domains. Furthermore, 6% micrograph(Figure 4.2) shows crosshatch patterns of CNC structures which is a indication of the liquid crystalline phase. The patterns form by a combination of several chiral nematic structures. According to the literature, crosshatch patterns form due to the repulsive interactions that cause immobilization of the system. Usually, these patterns can be observed at higher concentrations of CNC suspensions. Therefore, it can be concluded that 6wt% has a liquid crystalline phase comprised of chiral nematic structures[73].

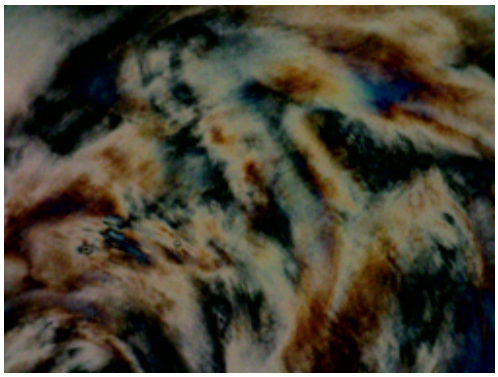

**Figure 4.1:** Yield Stress 4wt%

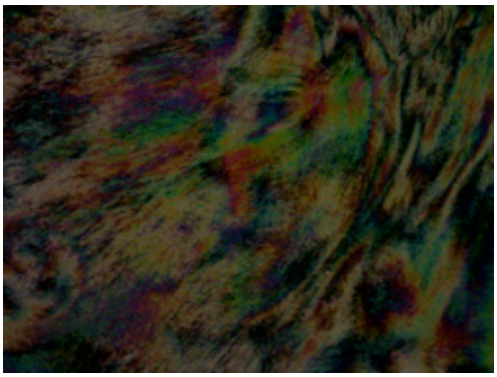

**Figure 4.2:** Yield Stress 6wt%

### 4.1.2 Rheo-PLI Results

#### 4.1.2.1 Yield Stress Tests

Yield stress tests were performed by applying shear stress in the stress range 0.1 – 100Pa at a constant time interval of 30s. The effect of shear stress at constant time can be evaluated by performing this test. All Rheo–PLI results obtained from the study are indicated as shown figure 4.3 and 4.4. Rheological responses and their corresponding PLI diagrams are indicated. The PLI diagram at the middle corresponds to the deformation over arc A-B while the PLI diagram at the bottom corresponds to the radial deformation[73].

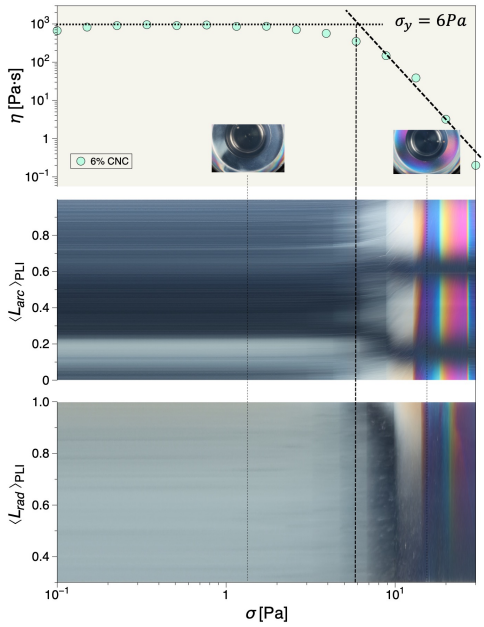


**Figure 4.3:** Yield Stress 6wt%

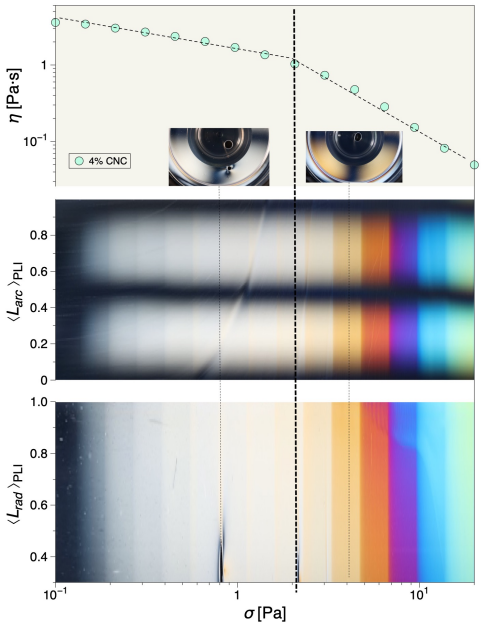


**Figure 4.4:** Yield Stress 4wt%

Figures 4.3 and 4.4 show the yield stress test results for 6wt% and 4wt% respectively. Yield stress is the stress at which viscosity begins to drop. Therefore yield stress of 6wt% is 6Pa. Below yield stress, no birefrigence patterns can be observed since the viscosity function is constant in this range. However, color changes can be seen slightly earlier than the yielding point of 6%. This could be due to rheometer is unable to capture the structural rearrangements occurs below yield stress. This could be attributed the Yielding can be clearly observed in both PLI diagrams of 6wt%. After yielding, significant birefringence can be observed due to the transition of random orientation of the CNC structure into flow-induced orientation. Since 6wt% consists of chiral nematic structures, during orientation these chiral nematic structures align towards the shear flow direction. However, very low extent of color changes can be seen slightly earlier than the yielding point of 6%. This could be due to the rheomter is unable to capture the structural rearrangements occurs below the yield stress. In both concentrations, at higher shear stress Maltese –Maltese-cross patterns were observed which is an indication of the predominant orientation of CNC structures towards shear flow.

Figure 4.4 shows the yielding behavior of 4wt% under the application of shear stress with constant time intervals. In PLI diagrams corresponding to 4wt%, equal time intervals can be clearly seen with different color distortions. Birefringence observed from the beginning of the test implies that the material has already yielded. In the rheological curve, two distinct regions of viscosity functions can be clearly observed. This behavior relates to the three-region viscosity behavior that has been mentioned in the literature. Kadar et al.(2023) has mentioned the three regions behavior of CNC structures in their suspensions[73]. According to the literature, three region viscosity functions are evidenced from biphasic and liquid crystalline systems. In region I, color patterns remain unchanged indicating that shear thinning during this region is associated to structural rearrangement below the observation scale.In contrast, with the increase of shear significant birefringence patterns observed in Region II due to orientation of structures.Therefore,the structural rearrangement associated with these two viscosity regions is attributed to orientation changes of two different length scales. Since 4% comprises both isotropic and liquid crystalline domains during the orientation at lower shear stresses CNC rods inside isotropic domains will align first and chiral nematic structures of liquid crystalline domains will start to align towards the shear flow direction with the increase of shear.

#### 4.1.2.2 Creep tests

Creep tests were performed by applying five different constant shear stresses over 1000s of time and viscosity function was measured. In this study, imposed shear stresses are larger, smaller, and near the yield stress of the respective CNC concnetration. The yield stress range was determined based on the yield stress test. Since 4wt% does not show yield stress at a given shear stress range we decided to choose 2.2Pa as the yield stress(Stress corresponds to separating line of two regions of yield stress test 4wt% as shown in Figure 4.4) to determine the yield stress range for the creep test. Yield stress range is higher than in liquid crystalline CNC suspensions (6wt%) compared with biphasic suspensions(4wt%). For 6wt% CNC suspensions, applied constant shear stresses are 5Pa,7Pa,15Pa,18Pa and 30Pa. For 4wt%, applied shear stresses are 0.1Pa,1Pa,3Pa,6Pa, and 10Pa.

As shown in Figure 4.5, in 6wt% CNC suspension, at 5Pa which is below yield stress, viscosity increases with observation time due to material build-up. CNC structures forms interactions with surrounding structures resulting viscosity an increase. Birefrigence observed within the time scale at this shear stress perhaps due to orientation towards shear flow. At 7Pa(near yield stress), color patterns remain unchanged which corresponds to constant viscosity function with time. Above yield stress(at 15Pa,18Pa, and 30pa), viscosity decreases over time due to material breakdown. Significant birefringence observed above yield stress since the material has started moving and they highly orients towards the shear flow. Considerable color transitions were observed and the transition region reduced with the increase of shear. The time required to achieve the steady state has decreased over the increase of shear stress. Increased shear stress first shifts the color from brown to violet then finally returns to green which is a lower wavelength color to higher wavelength colors. The increase in wavelengths could be attributed to the increase of the distance between the nematic structures[74].

As shown in Figure 4.6, in 4% CNC suspension, at 0.1Pa and 1Pa which is below yield stress, viscosity increases with time due to material restructure dominating over breakdown. Shear viscosity increases rapidly with time at 0.1Pa, but birefringence cannot be observed might be due to structural changes associated with the restructuring mainly involving CNC particles which can be captured by only rheology, not by the PLI patterns at the observation scale. Birefringence is observed in other shear stresses and the color transforms from lower wavelength colors to higher wavelength colors that provides an indication increase in the spacing between CNC structures with the increase of shear stress. Color transitions are not observed in this concentration hence structures do not experience yielding and any movement. 4wt% reaches the steady state earlier compared with 6wt%.As similar with 6wt%, the above yield stress viscosity increases with time due to material breakdown. With the increase in CNC concentration, shear viscosity shows higher values and more birefrigence is observed.

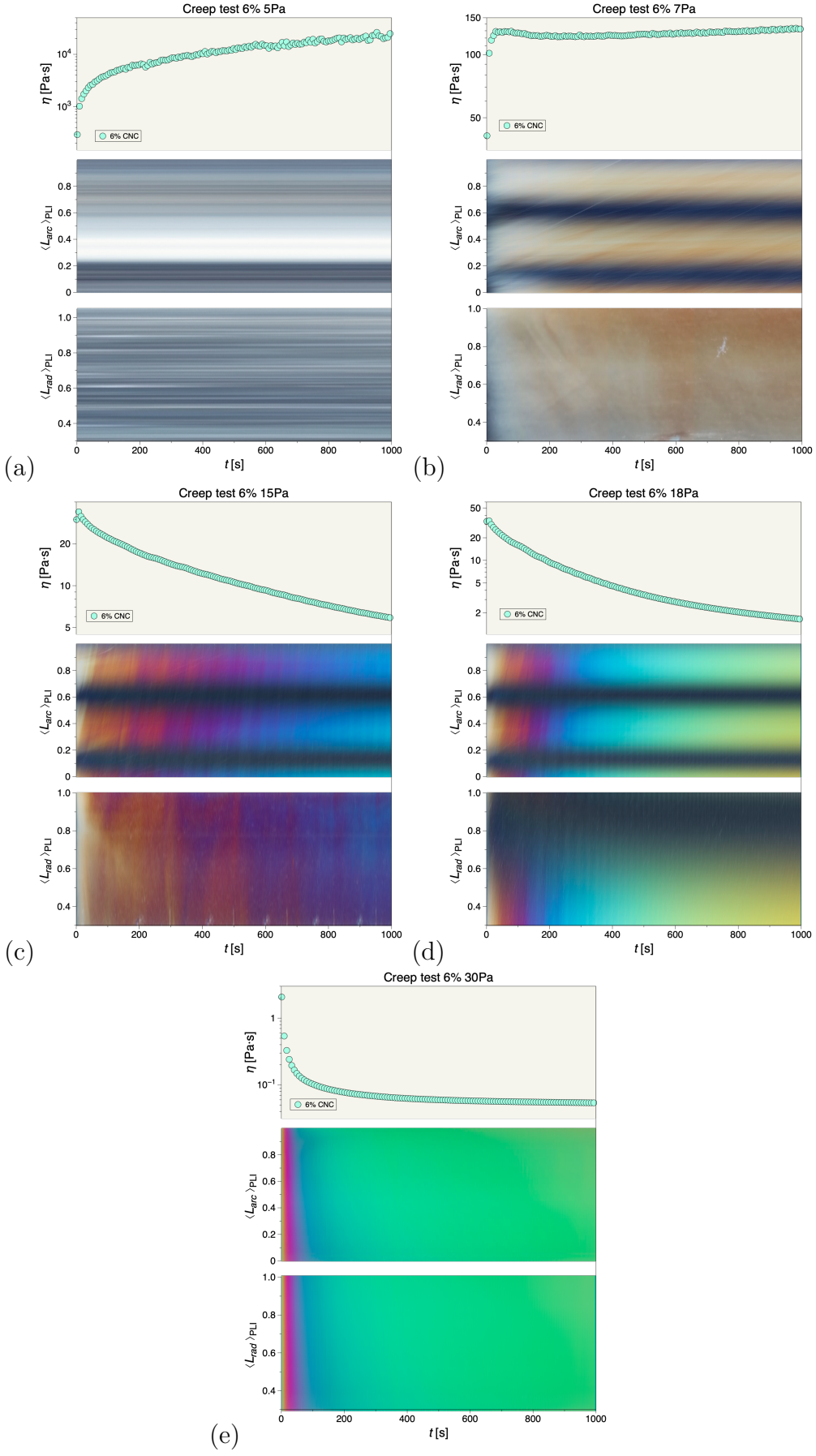


**Figure 4.5:** Creep test results 6 wt%(a)5Pa (b)7Pa (c)15Pa (d)18Pa (e)30Pa

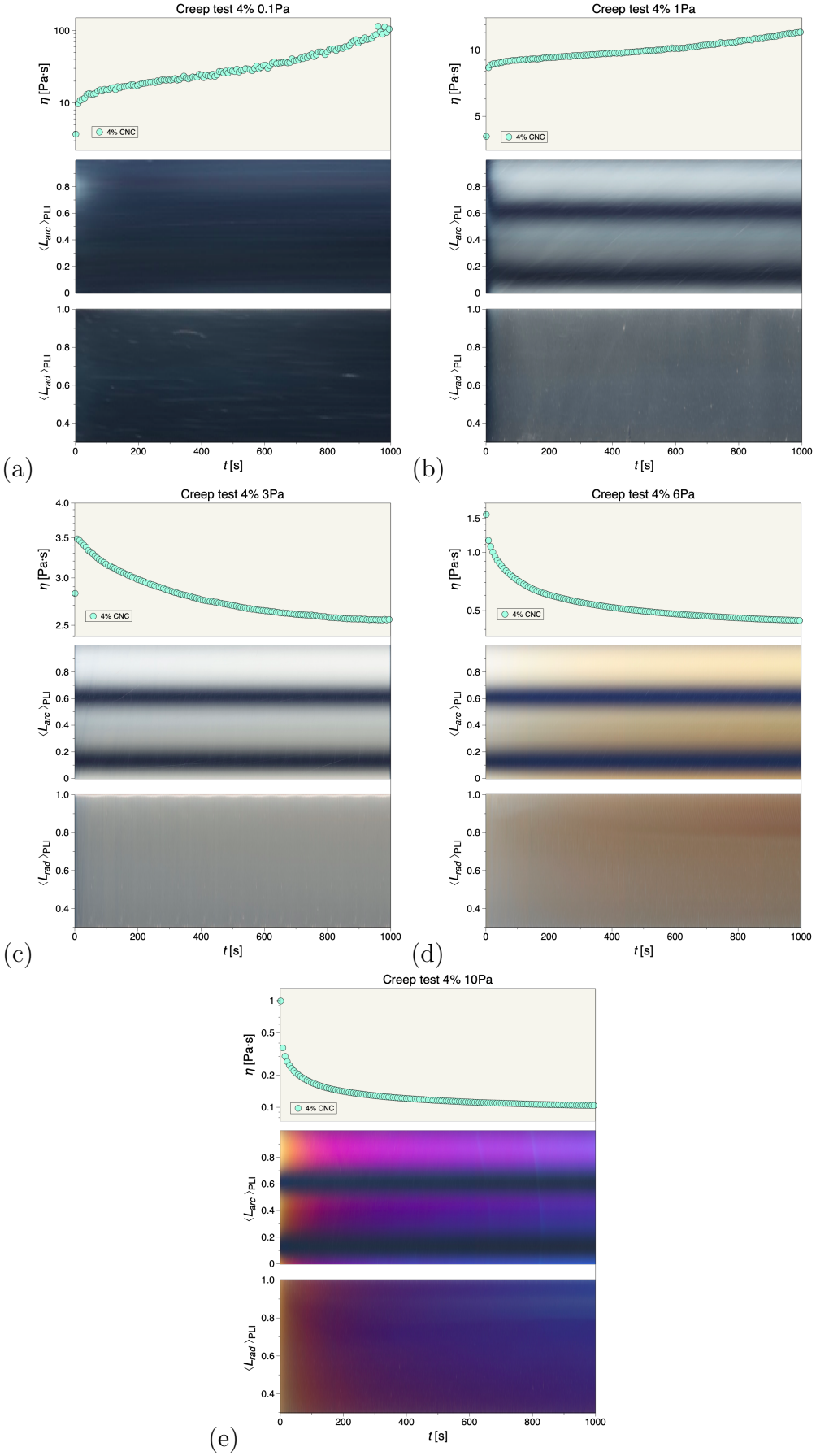


**Figure 4.6:** Creep test results 4 wt%(a)0.1Pa (b)1Pa (c)3Pa (d)6Pa (e)10Pa

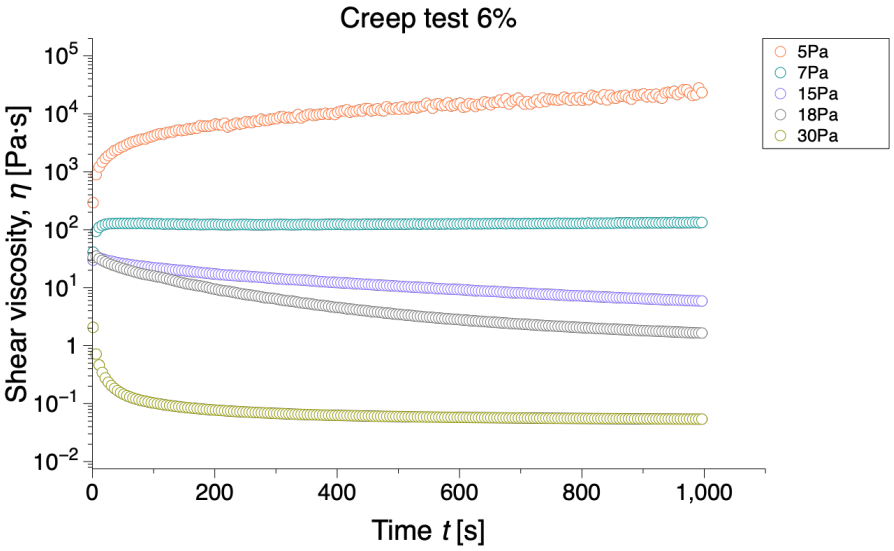


(a)

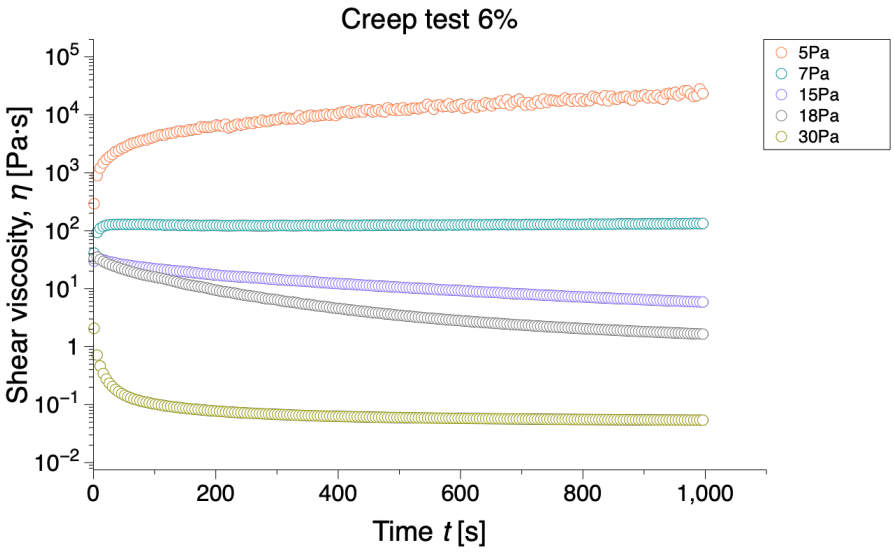


(b)

**Figure 4.7:** Creep curves (a)4 wt% (b)6 wt%

#### 4.1.2.3 Thixotropy Test

**Effect of Concentration**

Thixotropy behavior of CNC suspensions measured by performing hysterias loop test. The shear rate was ramped up and down in the range of 0.1 to 100 s-1 with a time step size of the 30s.

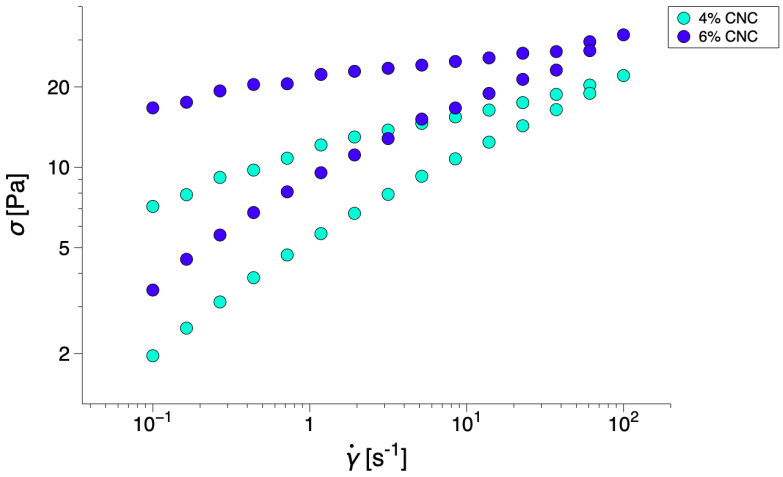


**Figure 4.8:** Hysteresis Curves

In this test, induced shear stress is measured with respect to the applied shear rate. During the upward sweep, the microstructure of the material disrupts at a higher shear rate and recovers back during the downward sweep. The area within the loop is the relative measure of thixotropy. This area can be calculated by integrating the stress in relation to the shear rate during the increase of the shear rate and subtracting the integrated stress in relation to the shear rate during the decrease of the shear rate.

$$A = \int_{t_0}^{t_{1/2}} \sigma d\dot{\gamma} - \int_{t/2}^{t_{end}} \sigma d\dot{\gamma} \tag{4.1}$$

The computed areas of hysterias loops of 4wt % and 6wt % are 212.38 and 364.26 suggesting that thixotropy increases with CNC concentration due to enhanced interactions. Domains uniformly orient towards the shear flow evidenced by Maltese cross patterns. Although 4wt% suspension does not consist of yield stress at a given shear rate range, it exhibits thixotropy behavior(Figure 4.9). As the shear rate and induced shear stress increase, CNC domains transition from random orientation to flow-induced orientation which corresponds to significant color transitions. Color transfers from violet to blue suggest that the distance between nematic structures increases with the increase of shear.

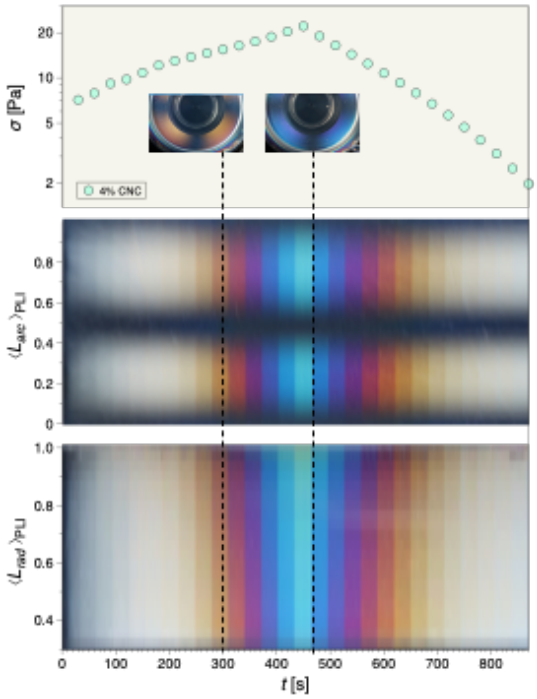


**Figure 4.9:** Thixotropy test 4wt%

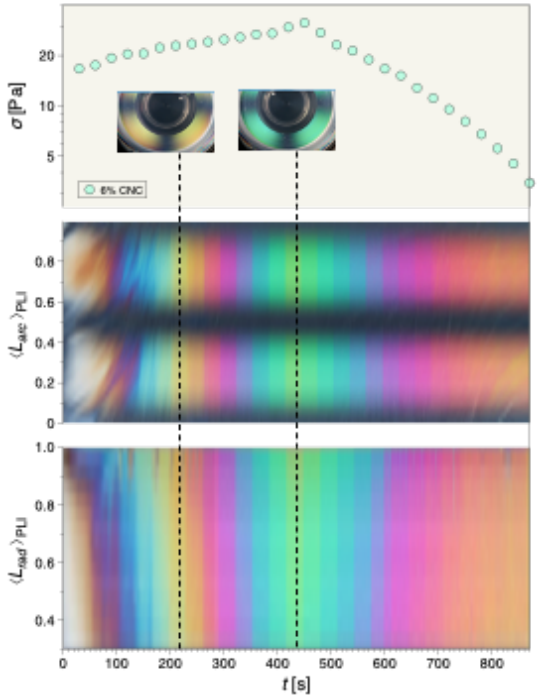


**Figure 4.10:** Thixotropy test 6wt%

In 6wt% suspension(Figure 4.10), yielding is clearly observed at the beginning of the test and more color patterns show with the increase of shear rate.More color distortions were observed due to the presence of more chiral nematic structures. Color patterns change from blue to green which is lower to higher wavelength colors. During the downward ramp, color transformation in 4% is almost the same as the upward ramp except for the fact that the color patterns do not return to the initiate state. In contrast,6wt% suspensions show a considerable difference in color transition during the downward ramp highlighting the fact that it has higher thixotropy.

### Effect of Time

To examine the effect of time on thixotropic behavior, the time step size was increased to 45s. In figure 4.11, the rheological state corresponds to the time at 350s has reached earlier in 45s. In contrast, 6wt% does not show any notable time effect as it has almost the same curves and PLI diagrams. The reason for that might be that 6wt% has reached the steady state at 30s.

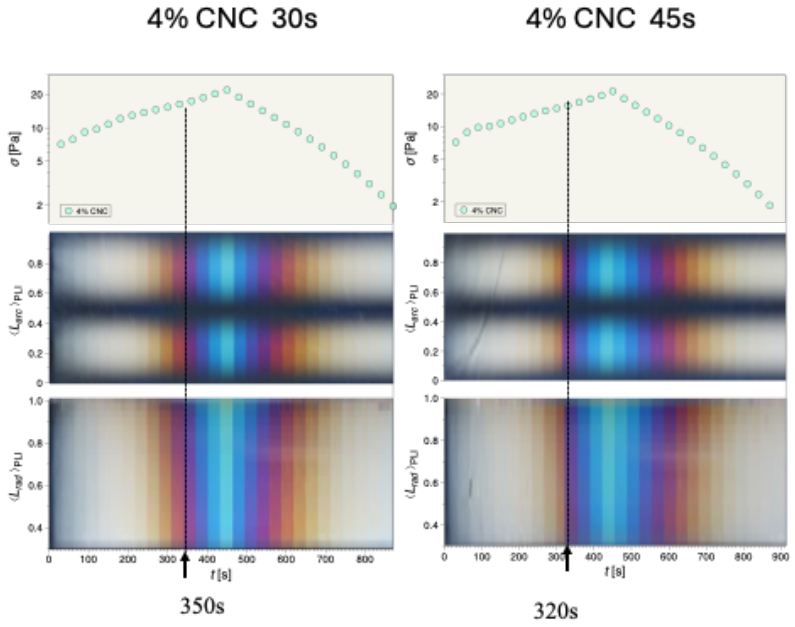


**Figure 4.11:** Thixotropy test at 30s and 45s 4wt%

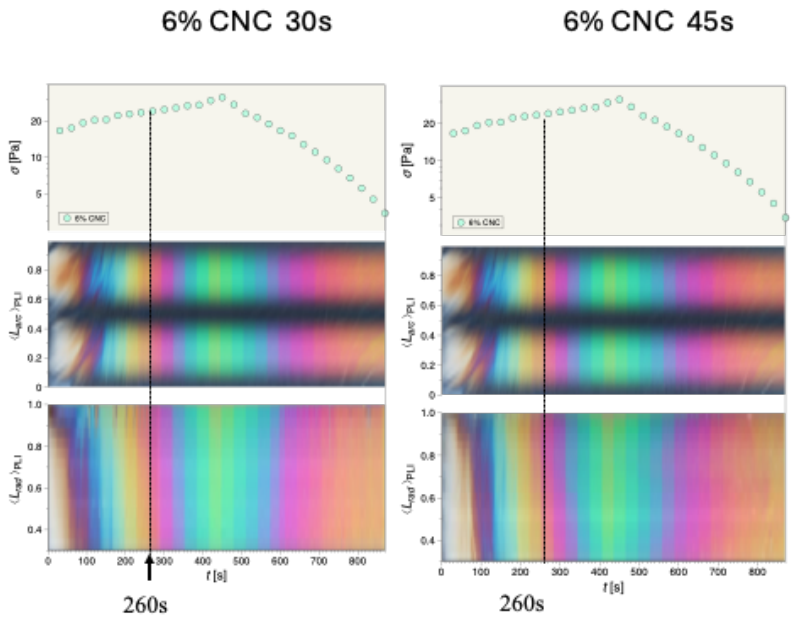


**Figure 4.12:** Thixotropy test at 30s and 45s 6wt%

#### 4.1.2.4 Oscillatory Shear Test

The viscoelastic behavior of CNC suspensions was determined by performing the oscillatory shear tests. In this analysis, shear strain was applied in the range of 0.001% to 1000% with a constant angular frequency of 1Hz. Figures 4.13 and 4.14 show the dynamic response of CNC suspensions 4wt% and 6wt% respectively. Curve is mainly divided into two main regions SAOS(Simple Amplitude Oscillatory Shear) and LAOS(Large Amplitude Oscillatory Shear).

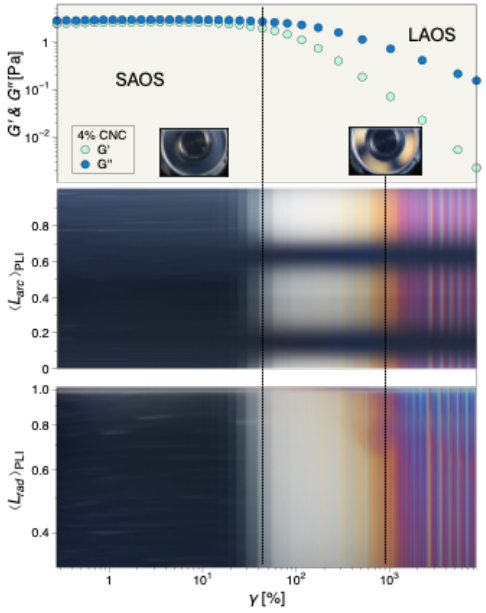


**Figure 4.13:** Oscillatory test 4wt%

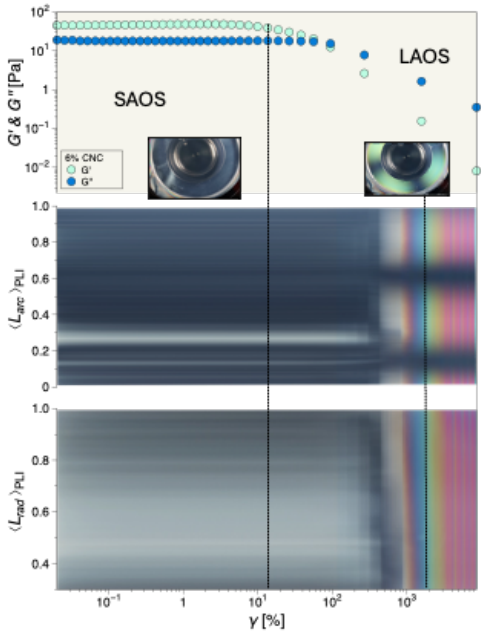


**Figure 4.14:** Oscillatory test 6wt%

As shown in Figure 4.13, 4wt% CNC suspension exhibits a fluid like behavior since G" > G' over the entire applied shear strain range. The dynamic response has a constant function during SAOS region might be due to the applied shear strain amplitude is not sufficient to rearrange the CNC structures. Nonlinear response of dynamic moduli observed in LAOS region which is corresponds to sudden change of birefrigence from SAOS to LAOS. At higher shear strains, more color patterns are observed in PLI diagram that depicts the occurrence of flow-induced orientation of CNC structures.

6wt% CNC suspension exhibits a gel-like behavior since G' > G" over the entire experiment time and G" increases at the transition to a nonlinear region(Figure 4.14). Birefringence is not observed until the material is subjected to higher shear strain. Towards very higher shear strains significant color transitions occurs which depicts the CNC structures align towards the shear flow and form higher spacings between nematic structures. When compared with 4wt% dynamic response, it shows a considerable reduction of dynamic moduli that might be due to the hydrogen bondings and networking in chiral nematic structures of 6 wt% which restricts

the angular movement.

# 5

# Conclusion

In this study, rheological measurements were performed by combining polarized light imaging to analyze the flow dynamics of CNC suspensions and simultaneous observation of the structure development of CNC assembly. In a yield stress test, we found out that 4wt% CNC suspensions do not show any yield stress in the given stress range. This finding highlights the importance of using polarized light imaging in combine with rheological measurements.

In creep tests, below yield stress material build-up dominates over break showing an increase of shear viscosity with time. In both cases, color patterns not observed below the yield stress. This could be attributed to the restruction being mostly associated with CNC particles rather than mesogens which cannot to make influence for bulk flow. In biphasic phase suspension(4wt%) this might be happen with the isotropic phase while in liquid crystalline phase(6wt%) might occur between the interface of mesogens. Above yield stress, destrution dominates over restruction showing a decrease of viscosity with time. The time required to achieve the steady state for 6wt% of the liquid crystalline phase is larger compared with 4wt%. Therefore, 4wt% has a higher stability with time compared to 6wt%.

Biphasic phase suspension of 4wt% has a fluid-like behavior and liquid crystalline phase of 6wt% shows a gel-like behavior with higher interactions and hydrogen bonding. Therefore, 6wt% exhibits a lower response of dynamic moduli than 4wt%. In both suspensions, significant color progressions were observed at higher shear strain amplitudes due to the orientation of CNC structures at higher strains. Thixotropy and material recovery proportional to the CNC concentration. 4wt% suspension shows an almost symmetrical PLI diagram that implies it has a higher material recovery. In contrast 6wt%, has a lower material recovery. Time has a considerable effect on the thixotropic behavior of 4wt% CNC suspension while 6wt% has a less effect.

The viscoelastic behavior of CNC suspensions was determined by performing oscillatory shear tests. 4wt% shows a liquid-like behavior where the medium (tap water in this project) predominantly influences the deformation under oscillation conditions, given the low particle content, which limits interactions between particles. In contrast, 6wt% shows a gel-like behavior where it consists of physical networking with higher interactions. Lower shear strain amplitude is not sufficient to rearrange the CNC structures in both suspensions. 6wt% shows birefrigence towards higher shear strain although dynamic moduli shows a reduction around middle shear strain values. This could be due to the CNC structure arrangement mostly associated with CNC particles rather than mesogens that can only be detected by rheological properties, not observable using polarized light imaging. By considering

all the promising results obtained from this study, we can conclude that rheo- PLI is a suitable method to analyze the rheological measurements and simultaneous observation of the development of CNC structures in their suspensions. This study includes valuable information about CNC rheological properties in their suspensions especially useful for applications such as 3D printing using CNC materials.

# Bibliography


[1] George,J.,& Sabapathi, S. N. (2015). Cellulose nanocrystals: synthesis, functional properties, and applications. Nanotechnology, science and applications, 45-54.

[2] Habibi, Y., Lucia, L. A., & Rojas, O. J. (2010). Cellulose nanocrystals: chemistry, self-assembly, and applications. Chemical reviews, 110(6), 3479-3500.

[3] Kádár, R., Spirk, S., & Nypelo, T. (2021). Cellulose nanocrystal liquid crystal phases: Progress and challenges in characterization using rheology coupled to optics, scattering, and spectroscopy. ACS nano, 15(5), 7931-7945.

[4] da Rosa, R. R., Silva, P. E., Saraiva, D. V., Kumar, A., de Sousa, A. P. M., Sebastião, P., ... & Godinho, M. H. (2022). Cellulose Nanocrystal Aqueous Colloidal Suspensions: Evidence of Density Inversion at the Isotropic-Liquid Crystal Phase Transition. Advanced Materials, 34(28), 2108227.

[5] Lagerwall, J. P., Schütz, C., Salajkova, M., Noh, J., Hyun Park, J., Scalia, G., & Bergström, L. (2014). Cellulose nanocrystal-based materials: from liquid crystal self-assembly and glass formation to multifunctional thin films. NPG Asia Materials, 6(1), e80-e80.

[6] Camarero Espinosa, S., Kuhnt, T., Foster, E. J., & Weder, C. (2013). Isolation of thermally stable cellulose nanocrystals by phosphoric acid hydrolysis. Biomacromolecules, 14(4), 1223-1230.

[7] Hirai, A., Inui, O., Horii, F., & Tsuji, M. (2009). Phase separation behavior in aqueous suspensions of bacterial cellulose nanocrystals prepared by sulfuric acid treatment. Langmuir, 25(1), 497-502.

[8] Almeida, A. P., Canejo, J. P., Fernandes, S. N., Echeverria, C., Almeida, P. L., & Godinho, M. H. (2018). Cellulose-based biomimetics and their applications. Advanced Materials, 30(19), 1703655.

[9] Wei, X., Lin, T., Duan, M., Du, H., & Yin, X. (2021). Cellulose Nanocrystal-based Liquid Crystal Structures and the Unique Optical Characteristics of Cellulose Nanocrystal Films. Bioresources, 16(1).

[10] Parker, R. M., Guidetti, G., Williams, C. A., Zhao, T., Narkevicius, A., Vignolini, S., & Frka-Petesic, B. (2018). The self-assembly of cellulose nanocrystals: Hierarchical design of visual appearance. Advanced Materials, 30(19), 1704477.

[11] Wei, G., Lu, M., Feng, K., Ma, S., Jiang, Y., & Jin, Z. (2023). Exploring the Core Parameters of CNC-Based Chiral Nematic Structures for Enhancing the Dissymmetry Factor of Right-Handed Circularly Polarized Luminescence. ACS omega, 8(25), 23191-23201.

[12] Wojno, S., Fazilati, M., Nypelö, T., Westman, G., & Kádár, R. (2022). Phase transitions of cellulose nanocrystal suspensions from nonlinear oscillatory shear. Cellulose, 29(7), 3655-3673.

[13] Kádár, R., Spirk, S., & Nypelo, T. (2021). Cellulose nanocrystal liquid crystal phases: Progress and challenges in characterization using rheology coupled to optics, scattering, and spectroscopy. ACS nano, 15(5), 7931-7945.

[14] Wojno, S., Ahlinder, A., Altskär, A., Stading, M., Abitbol, T., & Kádár, R. (2023). Percolation and phase behavior in cellulose nanocrystal suspensions from nonlinear rheological analysis. Carbohydrate Polymers, 308, 120622.

[15] Lane, C., Rode, D., & Rösgen, T. (2022). Birefringent properties of aqueous cellulose nanocrystal suspensions. Cellulose, 29(11), 6093-6107.

[16] Lane, C., Rode, D., & Rösgen, T. (2022). Birefringent properties of aqueous cellulose nanocrystal suspensions. Cellulose, 29(11), 6093-6107.

[17] Wei, G., Lu, M., Feng, K., Ma, S., Jiang, Y., & Jin, Z. (2023). Exploring the Core Parameters of CNC-Based Chiral Nematic Structures for Enhancing the Dissymmetry Factor of Right-Handed Circularly Polarized Luminescence. ACS omega, 8(25), 23191-23201.

[18] Frka-Petesic, B., Radavidson, H., Jean, B., & Heux, L. (2017). Dynamically controlled iridescence of cholesteric cellulose nanocrystal suspensions using electric fields.

[19] Abbasi Moud, A., & Abbasi Moud, A. (2022). Cellulose Nanocrystals (CNC) Liquid Crystalline State in Suspension: An Overview. Applied Biosciences, 1(3), 244-278.

[20] Haywood, A. D., & Davis, V. A. (2017). Effects of liquid crystalline and shear alignment on the optical properties of cellulose nanocrystal films. Cellulose, 24, 705-716.

[21] Wojno, S., Ahlinder, A., Altskär, A., Stading, M., Abitbol, T., & Kádár, R. (2023). Percolation and phase behavior in cellulose nanocrystal suspensions from nonlinear rheological analysis. Carbohydrate Polymers, 308, 120622.

[22] Wojno, S., Fazilati, M., Nypelö, T., Westman, G., & Kádár, R. (2022). Phase transitions of cellulose nanocrystal suspensions from nonlinear oscillatory shear. Cellulose, 29(7), 3655-3673.

[23] Kádár, R., Spirk, S., & Nypelo, T. (2021). Cellulose nanocrystal liquid crystal phases: Progress and challenges in characterization using rheology coupled to optics, scattering, and spectroscopy. ACS nano, 15(5), 7931-7945.

[24] Fazilati, M., Ingelsten, S., Wojno, S., Nypelö, T., & Kádár, R. (2021). Thixotropy of cellulose nanocrystal suspensions. Journal of Rheology, 65(5), 1035-1052.

[25] Anvari Ardakani, H. (2014). Rheology of pastes: effects of fibrillation, thixotropy and structure (Doctoral dissertation, University of British Columbia).

[26] Quanji, Z. (2010). Thixotropic behavior of cement-based materials: effect of clay and cement types. Iowa State University.

[27] Møller, P. C., Mewis, J., & Bonn, D. (2006). Yield stress and thixotropy: on the difficulty of measuring yield stresses in practice. Soft matter, 2(4), 274-283.

[28] Dullaert, K., & Mewis, J. (2006). A structural kinetics model for thixotropy. Journal of non-newtonian fluid mechanics, 139(1-2), 21-30.

[29] N'gouamba, E., Goyon, J., Tocquer, L., Oerther, T., & Coussot, P. (2020). Yielding, thixotropy, and strain stiffening of aqueous carbon black suspensions. Journal of Rheology, 64(4), 955-968.

[30] Mainardi, F., & Spada, G. (2011). Creep, relaxation, and viscosity properties for basic fractional models in rheology. The European Physical Journal Special Topics, 193(1), 133-160.

[31] Clain, F. M., Guilherme, C. E. M., Cardoso, F. B., Machado, F. M., Camaratta, R., Bergmann, C. P., & Osorio, A. G. (2023). Creep and electrical properties of carbon nanotube yarns for long-term applications. Carbon Trends, 13, 100313.

[32] Jaweej, M. J., Abdulhussein, M. A., & kassim Zalzala, B. (2014). Experimental and Numerical investigation of creep behavior in isotropic composites. Journal of Engineering, 20(1), 50-61.

[33] Jaweej, M. J., Abdulhussein, M. A., & kassim Zalzala, B. (2014). Experimental and Numerical investigation of creep behavior in isotropic composites. Journal of Engineering, 20(1), 50-61.

[34] Li, Y. L., Shen, M. Y., Chen, W. J., Chiang, C. L., & Yip, M. C. (2011). Creep Behavior and Mechanical Properties of Carbon Fiber Nano-Composites. Advanced Materials Research, 338, 156-165.

[35] Moud, A. A. (2023). CNC Gel Rheology Meets Mechanical Characteristics. In Advances in Rheology of Materials. IntechOpen.

[36] Song, H. Y., Park, S. J., & Hyun, K. (2023). Distinguishing between Linear and Star Polystyrenes with Unentangled Arms by Dynamic Oscillatory Shear Tests. ACS Macro Letters, 12(7), 968-973.

[37] Kodavaty, J., Pannala, R. P. K., Wasson, S., Mittal, M., Irshad, A. (2022, February). A novel method to choose the experimental parameters in large amplitude oscillatory shear rheology. In Materials Science Forum (Vol. 1048, pp. 54-64). Trans Tech Publications Ltd.

[38] Joyner, H. S. (2021). Nonlinear (large-amplitude oscillatory shear) rheological properties and their impact on food processing and quality. Annual review of food science and technology, 12, 591-609.

[39] Carrera, Y., Gonzalez, M., Rodriguez-Huezo, M. E., & Meraz, M. (2022). Large amplitude oscillatory shear (LAOS) rheology of candelilla wax/canola oil oleogels. Revista Mexicana de Ingeniería Química, 21(2), Bio2816-Bio2816.

[40] Danesh, M., Mauran, D., Hojabr, S., Berry, R., Pawlik, M., & Hatzikiriakos, S. G. (2020). Yielding of cellulose nanocrystal suspensions in the presence of electrolytes. Physics of Fluids, 32(9).

[41] Buffa, J. M., Casado, U., Mucci, V., & Aranguren, M. I. (2019). Cellulose nanocrystals in aqueous suspensions: rheology of lyotropic chiral liquid crystals. Cellulose, 26, 2317-2332.

[42] Zakani, B., Bose, A., & Grecov, D. (2024). Yield stress analysis of cellulose nanocrystals (CNCs) in hyaluronic acid suspensions. Carbohydrate Polymers, 326, 121650.

[43] Barnes, H. A., Hutton, J. F., & Walters, K. (1989). An introduction to rheology (Vol. 3). Elsevier.

[44] Zakani, B., & Grecov, D. (2020). Yield stress analysis of cellulose nanocrystalline gels. Cellulose, 27, 9337-9353.

[45] Ferrás, L. L., & Afonso, A. M. (2023). Viscoelasticity: Mathematical Modelling, Numerical Simulations, and Experimental Work. Applied Sciences, 13(2), 1022.

[46] Tecse, A., Romero, S. E., Naemi, R., & Castaneda, B. (2023). Characterization of the soft tissue viscous and elastic properties using ultrasound elastography and rheological models: validation and applications in plantar soft tissue assessment. Physics in Medicine  Biology, 68(10), 105005.

[47] Beber, V. C., Schneider, B., & Brede, M. (2016). Influence of temperature on the fatigue behaviour of a toughened epoxy adhesive. The Journal of Adhesion, 92(7-9), 778-794.

[48] Hyun, K., & Wilhelm, M. (2018). Nonlinear oscillatory shear mechanical responses. Nonlinear dielectric spectroscopy, 321-368.

[49] Yan, B., Ren, J., Zheng, X., Liu, Y., & Zou, Q. (2017). High-speed broadband monitoring of cell viscoelasticity in real time shows myosin-dependent oscillations. Biomechanics and Modeling in Mechanobiology, 16, 1857-1868.

[50] Le Guisquet, S., & Amabili, M. (2023). Identification of the viscoelastic properties of a hydrogel in sol–gel transition by vibration experiments. Journal of the Mechanics and Physics of Solids, 171, 105152.

[51] Wei, L. (2023). Thixotropic cement slurry system types and evaluation methods. International Journal of New Developments in Engineering and Society, 7(1).

[52] Bhattacharyya, T., Jacob, A. R., Petekidis, G., & Joshi, Y. M. (2023). On the nature of flow curve and categorization of thixotropic yield stress materials. Journal of Rheology, 67(2), 461-477.

[53] Wang, Y., & Ewoldt, R. H. (2022). Distinguishing thixotropy, anti-thixotropy, and viscoelasticity using hysteresis. arXiv preprint arXiv:2212.07572.

[54] El Bitouri, Y., & Azéma, N. (2022). On the "Thixotropic" Behavior of Fresh Cement Pastes. Eng, 3(4), 677-692.

[55] Sen, S., & Ewoldt, R. H. (2022). Thixotropic spectra and Ashby-style charts for thixotropy. Journal of Rheology, 66(5), 1041-1053.

[56] Sen, S., & Ewoldt, R. H. (2022). Thixotropic spectra and Ashby-style charts for thixotropy. Journal of Rheology, 66(5), 1041-1053.

[57] Raheena, M., & Robinson, R. G. (2022). Determining the strain rate of controlled-strain loading consolidation test with hydraulic conductivity. Canadian Geotechnical Journal, 60(7), 1073-1078.

[58] Raheena, M., & Robinson, R. G. (2022). Determining the strain rate of controlled-strain loading consolidation test with hydraulic conductivity. Canadian Geotechnical Journal, 60(7), 1073-1078.

[59] Kouřilová, V., Dufková, R., Hřivna, L., & Kumbár, V. (2022). Use of rheological plastic models to describe the flow behavior of unconventional chocolate masses. Czech Journal of Food Sciences, 40(4).

[60] Bui, C., & Ho, T. (2021, November). Effects of the regularization parameter on the flow characteristics of a viscoplastic fluid. In AIP Conference Proceedings (Vol. 2420, No. 1). AIP Publishing.

[61] Ellwanger, F., Georgantopoulos, C. K., Karbstein, H. P., Wilhelm, M., & Azad Emin, M. (2023). Application of the ramp test from a closed cavity rheometer to obtain the steady-state shear viscosity  (). Applied Rheology, 33(1), 20220149.
[62] Tardani, F., La Mesa, C., Poulin, P., & Maugey, M. (2012). Phase behavior of DNA-based dispersions containing carbon nanotubes: effects of added polymers and ionic strength on excluded volume. The Journal of Physical Chemistry C, 116(18), 9888-9894.
[63] Kádár, R., Spirk, S., & Nypelo, T. (2021). Cellulose nanocrystal liquid crystal phases: Progress and challenges in characterization using rheology coupled to optics, scattering, and spectroscopy. ACS nano, 15(5), 7931-7945.
[64] Kádár, R., Fazilati, M., & Nypelö, T. (2020). Unexpected microphase transitions in flow towards nematic order of cellulose nanocrystals. Cellulose, 27, 2003-2014.
[65] Le Kien, F., Nic Chormaic, S., & Busch, T. (2023). Direction-dependent coupling between a nanofiber-guided light field and a two-level atom with an electric quadrupole transition. Physical Review A, 107(1), 013713.
[66] Mondal, P. P. (2022). Electromagnetic Optics and Polarization of Light. In Classical and Quantum Optics (pp. 4-1). Melville, New York: AIP Publishing LLC.
[67] Rodger, A., & Chubb, J. J. (2006). Circular dichroism and linear dichroism. Encyclopedia of Analytical Chemistry: Applications, Theory and Instrumentation, 1-42.
[68] Stafeev, S. S., Nalimov, A. G., Kovalev, A. A., Zaitsev, V. D., & Kotlyar, V. V. (2022, March). Circular polarization near the tight focus of linearly polarized light. In Photonics (Vol. 9, No. 3, p. 196). MDPI.
[69] Huang, X., Gao, H., He, J., Li, X., Li, X., Fan, J., & Guo, L. (2022). Broadband linear polarizer with highly efficient asymmetric transmission using a chiral metasurface. AEU-International Journal of Electronics and Communications, 152, 154244.
[70] Wang, J., Tan, X., Qi, P., Wu, C., Huang, L., Xu, X., ... & Kuroda, K. (2022). Linear polarization holography. Opto-Electronic Science, 1(2), 210009-1.
[71] Kádár, R., Fazilati, M., & Nypelö, T. (2020). Unexpected microphase transitions in the flow towards nematic order of cellulose nanocrystals. Cellulose, 27, 2003-2014.
[72] Kádár, R., Fazilati, M., & Nypelö, T. (2020). Unexpected microphase transitions in flow towards nematic order of cellulose nanocrystals. Cellulose, 27, 2003-2014.
[73] Wojno, S., Ahlinder, A., Altskär, A., Stading, M., Abitbol, T., & Kádár, R. (2023). Percolation and phase behavior in cellulose nanocrystal suspensions from nonlinear rheological analysis. Carbohydrate Polymers, 308, 120622.
[74] Fazilati, M., Ingelsten, S., Wojno, S., Nypelö, T., & Kádár, R. (2021). Thixotropy of cellulose nanocrystal suspensions. Journal of Rheology, 65(5), 1035-1052.

**DEPARTMENT OF SOME SUBJECT OR TECHNOLOGY**
**CHALMERS UNIVERSITY OF TECHNOLOGY**
Gothenburg, Sweden
www.chalmers.se


CHALMERS
UNIVERSITY OF TECHNOLOGY